Electrochimica Acta 191 (2016) 62–69

Contents lists available at ScienceDirect

Electrochimica Acta

journal homepage: www.elsevier.com/locate/electacta

Investigation of the role of Mn dopant in CdS quantum dot sensitized solar cell

Ting Shen[a], Jianjun Tian[a,*], Lili Lv[a], Chengbin Fei[b], Yajie Wang[b], Tönu Pullerits[c], Guozhong Cao[b,d,*]

[a] Institute of Advanced Materials and Technology, University of Science and Technology Beijing, Beijing, 100083, China
[b] Beijing Institute of Nanoenergy and Nanosystems, Chinese Academy of Sciences 100083, China
[c] Department of Chemical Physics, Lund University, Lund 22100, Sweden
[d] Department of Materials and Engineering, University of Washington, Seattle, WA, 98195-2120, USA

ARTICLE INFO

Article history:
Received 26 November 2015
Received in revised form 7 January 2016
Accepted 7 January 2016
Available online 11 January 2016

Keywords:
CdS
Quantum dot sensitized solar cells
Mn
Efficiency

ABSTRACT

Mn-doping into CdS quantum dots (QDs) has been demonstrated a useful way to enhance the power conversion efficiency (PCE) of quantum dot sensitized solar cells (QDSCs), the detailed systematic study is needed to get a better fundamental understanding. This work focuses on the study of the effects of Mn dopant on light harvesting, charge transfer, and charge collection of the solar cells. The results indicate that the Mn-doping into CdS QDs increases the light absorbance and extends the light absorption range, which results in the enhancement of the photo-generated current density. In addition, both the electron transport rate and the electron diffusion length are also increased with the introduction of Mn dopant. So the charge collection efficiency (η_{cc}) of the solar cell increases from 89.9% for CdS sample to 96.7% for Mn/CdS sample. As a result, the PCE of Mn/CdS QDSC reaches 3.29%, which is much higher than that of CdS QDSC (2.01%).

1. Introduction

Semiconductor quantum dots (QDs) based on II-VI group [1] such as CdSe [2], CdS [3], PbS [4,5], PbSe [6], ZnS [7] and CdSe/CdS [8], have an extensive use involved lasers [9], photocatalysis [10] and solar cells [11,12] due to the tunable band-gaps [13], high extinction coefficient [14], large intrinsic dipolar moment [15] and direct hot carrier transfer [16]. Additionally, owing to the multiple excition generation (MEG) [17–19], the theoretical power conversion efficiency (PCE) of the solar cells based QDs can reach up to 44%, which is much higher than that of 31% for semiconductor solar cells according to Schockley-Queisser limit [20,21]. Quantum dot sensitized solar cell (QDSC) is considered as one of the next generation solar cells, which has drawn a tremendous attention due to the simple and low-cost solution processed manufacture compared to the traditional silicon solar cells [22–24]. The typical structure of QDSCs is composed of a wide-band-gap mesoporous photoanodes (TiO_2 or SnO), narrow band-gap QDs as sensitizers, polysulfide electrolyte (S^{2-}/S_n^{2-}) and counter electrode (e.g. Cu_2S). During operation, the photons are harvested by QDs, generating the excitions (electron-hole pairs) that are rapidly separated into electrons and holes at the interface between photoanode and QDs. The electrons are transferred by photoanode, at same time, the holes are released by redox couples in the liquid electrolyte [25]. However, the observed efficiency of QDSCs is still very low, which may be attributed to the insufficient amount of QDs [26], serious surface charge recombination [27] and inappropriate internal band-gap structure [1,28].

In recent years, many researchers have devoted to the study of how to improving the PCE of QDSCs. Pan et al. [29] combined both advantages of CdSe and CdS in light harvesting and electron injection to prepare type-I CdS/CdSe core/shell structure QD-based solar cells, the efficiency of which reached 5.36%. Radich et al. [30] designed a Cu_2S/graphene oxide-based counter electrode for high efficiency QDSCs greater than 5% of PCE. Tian et al. [31–33] introduced the surface modification of photoanodes to reduce the charge recombination. Recently, the breakthrough revolution in QDSCs was made by Santra et al. using Mn dopant into CdS QD [34]. The PCE of CdS/CdSe QDSC was up to 5.4%. Subsequently, Tian et al. [35] doped Mn^{2+} into CdSe QDs to assemble $Cd_{1-x}Mn_xSe$ solar cells, which showed high efficiency (6.33%). Kim et al. [36] also doped Mn^{2+} into CdS for improving the performance of QDSCs. So doping transition metal ions is thought to be a useful way for designing highly efficiency solar cells. However, detailed systematic study on

* Corresponding author.
E-mail address: tianjianjun@mater.ustb.edu.cn (J. Tian).

http://dx.doi.org/10.1016/j.electacta.2016.01.056
0013-4686/

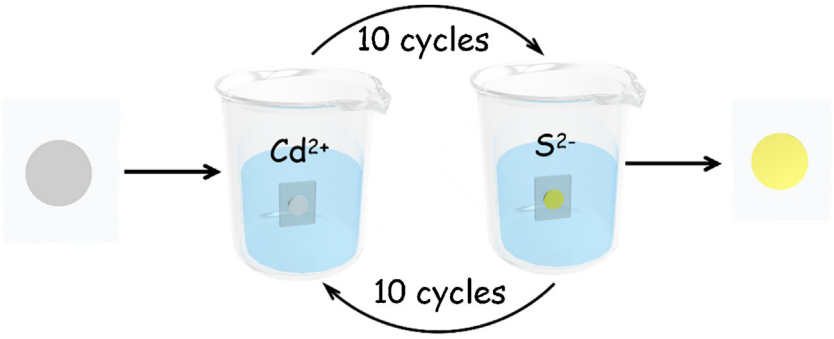

Scheme 1. Successive ionic layer absorption and reaction process.

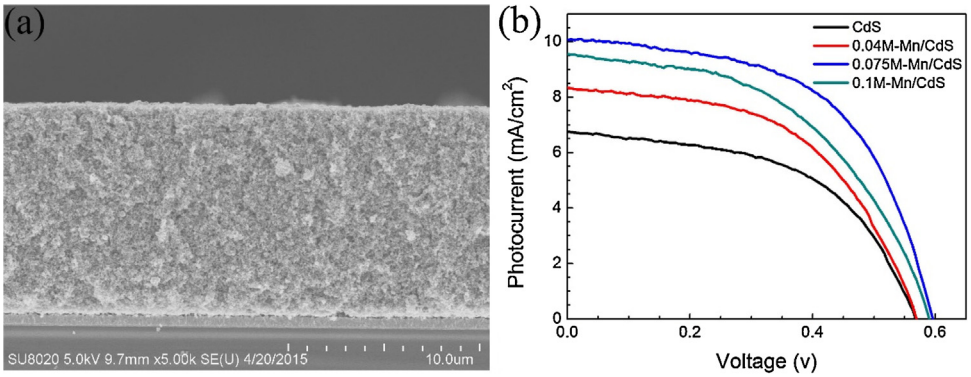

Fig. 1. (a) SEM image of cross section of the TiO_2 film, (b) Photocurrent density-voltage (*J-V*) curves of QDSCs assembled with undoped and Mn-doped CdS QDs, respectively. The *J-V* curves were measured under AM 1.5 G, at 1 sun light intensity with a shadow mask. The concentrations of Mn^{2+} dopant were 0, 0.04 M, 0.075 M and 0.1 M.

the effect of Mn dopant into CdS QD on the QDSC seems to be rarely reported. Therefore, investigation the role of Mn dopant into CdS QD should be explored.

Here, CdS QDs directly grow on the mesoporous TiO_2 film using successive ionic layer absorption and reaction (SILAR) as shown in Scheme 1. Cd^{2+} are adsorbed on the surface of TiO_2 nanoparticles at the first dipping step in the metallic precursor solution. After washing, Cd^{2+} reacts with S^{2-} to form CdS QD into the TiO_2 film at the second dipping step in the sulphur precursor solution. To achieve Mn doped CdS QD, the metallic precursor solutions are consisted of 0.04 M, 0.075 M and 0.1 M manganese acetate and 0.1 M cadmium nitrate aqueous solution, respectively. Our investigation reveals that the optimum amount of Mn-doped into CdS is 0.075 M, and the transition metal Mn^{2+} dopant into CdS can strongly improve the incident photon to charge carrier efficiency (IPCE), owing to the increased light harvesting, electron injection and charge collection efficiencies. As a result, the PCE of Mn/CdS QDSC is up to 3.29% under standard simulated AM 1.5 G, 100 mW/cm^2, which is much higher than that of QDSC without doping (2.01%).

Table 1
Amount of elements on the surface of the photoanodes assembled with CdS and Mn/CdS QDs determined from EDS.

Samples	Atomic %				
	O	Ti	Cd	S	Mn
CdS	64.968	28.134	3.356	3.542	0
0.04M-Mn/CdS	65.203	28.011	2.567	3.630	0.589
0.075M-Mn/CdS	65.142	28.216	2.173	3.622	0.847
0.1M-Mn/CdS	65.046	27.946	2.463	3.629	0.916

2. Experimental section

2.1. Materials

Cadmium nitrate tetrahydrate ($Cd(NO_3)_2{\cdot}4H_2O$, Alfa Aesar, 98.5%), sodium sulfide nonahydrate ($Na_2S{\cdot}9H_2O$, aladdin, ≥98.0%), manganese(II) acetate anhydrous ($Mn(CH_3COO)_2$, Alfa Aesar, 98%), zinc nitrate hexahydrate ($Zn(NO_3)_2{\cdot}6H_2O$, aladdin, 99%), sublimed sulfur (S, Guoyao China, ≥99.5%), hydrochloric acid (HCl, Beijing China, 36%-38%), methanol anhydrous (CH_3OH, Guoyao China, ≥99.5%), TiO_2 (Degussa P25). All of the chemicals without further purification to use directly.

2.2. Preparation of TiO_2 film

The porous TiO_2 films were prepared by our previously reported method [25]. In brief, the well-clean fluorine-doped tin oxide (FTO, 8 Ω/square) glass was used as substrate for the photoanode and fabricated by TiO_2 pastes which composed of TiO_2 nanoparticles, ethyl cellulose and α–terpineol, via the doctor blade method at

Table 2
Photovoltaic properties obtained from the *J-V* curves using undoped and Mn-doped CdS QDs as sensitizers.

Samples	V_{oc} (V)	J_{sc} (mA/cm^2)	FF	PCE (%)
CdS	0.57 ± 0.01	6.73 ± 0.33	0.52 ± 0.02	2.01 ± 0.24
0.04 M-Mn/CdS	0.57 ± 0.01	8.29 ± 0.41	0.53 ± 0.01	2.45 ± 0.15
0.075 M-Mn/CdS	0.60 ± 0.01	10.07 ± 0.39	0.55 ± 0.01	3.29 ± 0.19
0.1 M-Mn/CdS	0.59 ± 0.01	9.55 ± 0.44	0.49 ± 0.03	2.78 ± 0.22

Table 3
Electrochemical impedance results of QDSCs assembled with CdS and 0.075 M-Mn/CdS QDs, respectively.

Samples	R_c (Ω)	R_{ct} (Ω)	τ_r (s)
CdS	10.2	68.5	0.17
0.075 M-Mn/CdS	10.5	80.5	0.21

room temperature for 30 min followed by sintering process in air at 500 °C (2 °C/min) for 30 min.

2.3. Preparation of CdS QD

The SILAR method was used to deposit QDs on the TiO_2 photoanodes. In a typical synthesis protocol, the working electrodes were soaked in the cation and anion solutions for 1 min each solution, then rinsed with methanol and dried with air in between each step. Stock solutions of Cd^{2+} and S^{2-} were prepared from 0.1 M $Cd(NO_3)_2{\cdot}4H_2O$ in methanol and 0.1 M $Na_2S{\cdot}9H_2O$ in 1:1 methanol and water solution, respectively. To incorporate the doping of Mn^{2+}, 0.04 M, 0.075 M and 0.1 M $Mn(CH_3COO)_2$ methanol solutions were prepared and then mixed with $Cd(NO_3)_2{\cdot}4H_2O$, respectively. Generally, 10 cycles of SILAR process were repeated to deposit sufficient QDs on the TiO_2 films.

2.4. Preparation of ZnS Passivating Layer

The passivating layer of ZnS was made by SILAR method. The QD-deposited TiO_2 films were immersed into 0.1 M $Zn(NO_3)_2{\cdot}6H_2O$ and 0.1 M $Na_2S{\cdot}9H_2O$ solution for 1 min, respectively. The sulfur ion precursor was prepared by dissolving $Na_2S{\cdot}9H_2O$ in methanol and water solution with ratio of 1:1. The zinc ion precursor was prepared by dissolving $Zn(NO_3)_2{\cdot}6H_2O$ in methanol. The films were washed with methanol and dried with air. A total of 2 cycles of SILAR process were done in all the cases.

2.5. Counter electrode and electrolyte

In this study, compact Cu_2S film was used as the counter electrode. In a typical procedure, brass foils were immersed in 35%-38% HCl at 70 °C for 20 min, then washed with deionized water and dried in air. The etched brass foils were dipped into polysulfide electrolyte to form compact Cu_2S film. The electrolyte was prepared from 1.0 M S and 1.0 M Na_2S solution dissolved in 7:3 methanol-water solution.

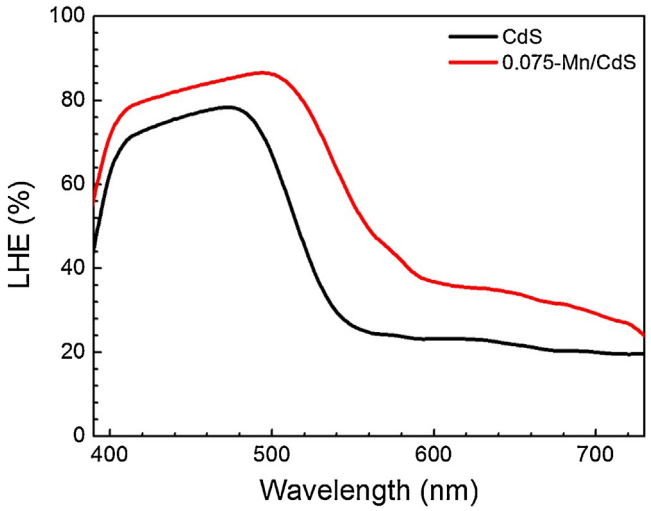

Fig. 3. Light Harvesting Efficiency (LHE) curves of the TiO_2 films loaded with CdS and 0.075 M-Mn/CdS QDs, respectively.

2.6. Characterization

Hitachi SU8020 SEM system equipped with an energy-dispersive X-ray spectroscope (EDS) operated at 20 KV was employed to analyze the thickness and the elemental composition of the film. The absorption spectra were recorded on a UV-visible spectrophotometer (Shimadzu UV-3600). The photoluminescence (PL) spectra were measured on Shimadzu luminescence spectrometer RF-5301PC. The active area of the QDSCs was 0.196 cm^2. The photovoltaic characteristics of the solar cells were evaluated using simulated AM 1.5 sunlight with an output power of 100 mW/cm^2. Incident photon to charge carrier efficiency (IPCE) spectra were obtained in the range 400–700 nm using a Keithley 2000 multimeter with illumination of a 300 W tungsten lamp with a Spectral Product DK240 monochromator. The electrochemical impedance spectroscopy (EIS) was carried out with an impedance analyzer (ZAHNER CIMPS) at forward bias -0.6 V over the frequency of 0.1 Hz to 100 kHz under dark condition.

3. Results and Discussion

Fig. 1(a) shows the scanning electron microscropy (SEM) image of cross section of TiO_2 film. It is clear that the thickness of the film

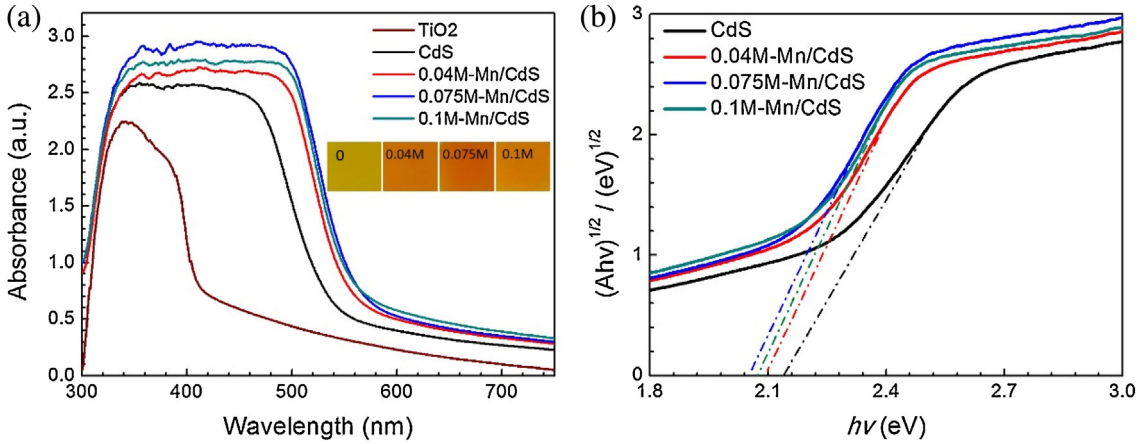

Fig. 2. (a) UV-visible spectral curves (inset shows the photographs of CdS and Mn/CdS photoanodes) and (b) $(Ah\nu)^{1/2}$ vs. $h\nu$ curves of TiO_2 films loaded with undoped and Mn-doped CdS QDs, respectively.

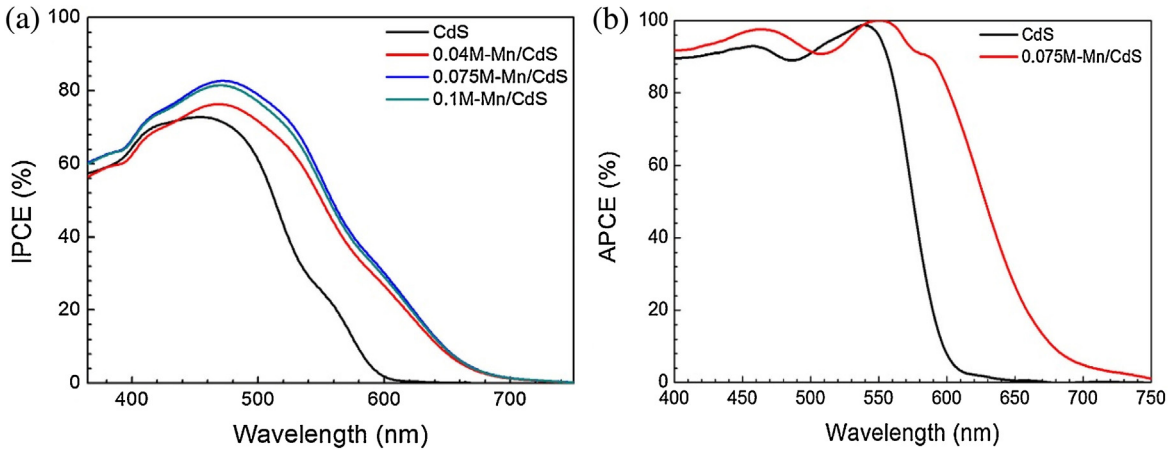

Fig. 4. (a) Incident photon to charge carrier efficiency (IPCE) spectra curves and (b) absorbed photon to current conversion efficiency (APCE) curves of QDSCs assembled with undoped and Mn-doped CdS QDs, respectively.

is 10–12 μm. According to our previous work [25]. the thickness of the TiO_2 film prepared using commercial P25 nanoparticles in around 11 μm exhibited the best performance for QDSC. We prepared Mn/CdS QDs sensitized photoanodes using different concentrations of Mn^{2+} precursor solution. Energy-dispersive X-ray (EDS) was conducted to monitor the elemental compositions of CdS and Mn/CdS QDs sensitized TiO_2 photoanodes as shown in Table 1. It can be seen that the amount of the Mn element in the Mn/CdS QDs sensitized TiO_2 photoanodes increases as Mn^{2+} solution concentration increases. The content of Cd element decreases accordingly. Fig. 1(b) shows the *J-V* characteristics of the QDSCs based on CdS, 0.04 M Mn^{2+} doped CdS (0.04 M-Mn/CdS), 0.075 M Mn^{2+} doped CdS (0.075 M-Mn/CdS), and 0.1 M Mn^{2+} doped CdS (0.1 M-Mn/CdS). The corresponding parameters of the solar cells including open circuit voltage (V_{oc}), short circuit current density (J_{sc}), fill factor (FF) and power conversion efficiency (PCE) are summarized in Table 2. In comparison to the QDSCs assembled with CdS QDs, it is clear that the Mn doped CdS-QDSCs exhibit significant improvement in the PCE. With increasing the concentration of Mn^{2+} precursor solution, both J_{sc} and PCE drastically increase to 8.29 mA/cm^2 and 2.45% for 0.04 M-Mn/CdS, and further to 10.07 mA/cm^2 and 3.29% for 0.075 M-Mn/CdS, and then decrease to 9.55 mA/cm^2 and 2.78% for 0.1 M-Mn/CdS. V_{oc} and FF of the solar cells show the same trend like J_{sc} and PCE. Among the properties of QDSCs, the increment of J_{sc} is highest, which is increased by 50% in comparison with CdS QDSC. J_{sc} is mainly affected by the number of the excited electron, electronic injection rate and electronic transport rate, which is expressed by the following equation [37]:

$$J_{sc} = (\mathrm{LHE}\cdot\Phi_{inj}\cdot\eta_{cc})\cdot\lambda\cdot P_{in(\lambda)}/1024 \quad (1)$$

where LHE is the light harvesting efficiency, Φ_{inj} is the electron injection efficiency, η_{cc} is the electron collection efficiency, λ is the absorbing wavelength, $P_{in(\lambda)}$ is the light intensity. The effects of Mn dopant on the LHE, Φ_{inj} and η_{cc} have been studied as following discussion.

The absorption spectra of the CdS and Mn/CdS QD-sensitized photoanodes are shown in Fig. 2(a). The absorption onsets are 545 nm, 575 nm, 585 nm and 585 nm for CdS, 0.04 M-Mn/CdS, 0.075 M-Mn/CdS and 0.1 M-Mn/CdS photoanodes, respectively. The absorbance of photoanodes increases as the concentration of Mn^{2+} precursor solution increases. When the concentration of Mn^{2+} precursor solution is more than 0.075 M, the absorbance of photoanodes decreases slightly. The inset in Fig. 2(a) displays the color of Mn/CdS QD films is much darker than that of CdS films, indicating that the more amounts of QDs is absorbed. High absorbance of the photoanodes means high loading amount of QDs according to the previous reports [36,38]. So the enhanced absorbance value of Mn/CdS compared to CdS will be ascribed to a greater amount of QDs into the TiO_2 films. However, the EDS results do not seem to support increased CdS QDs loading in the

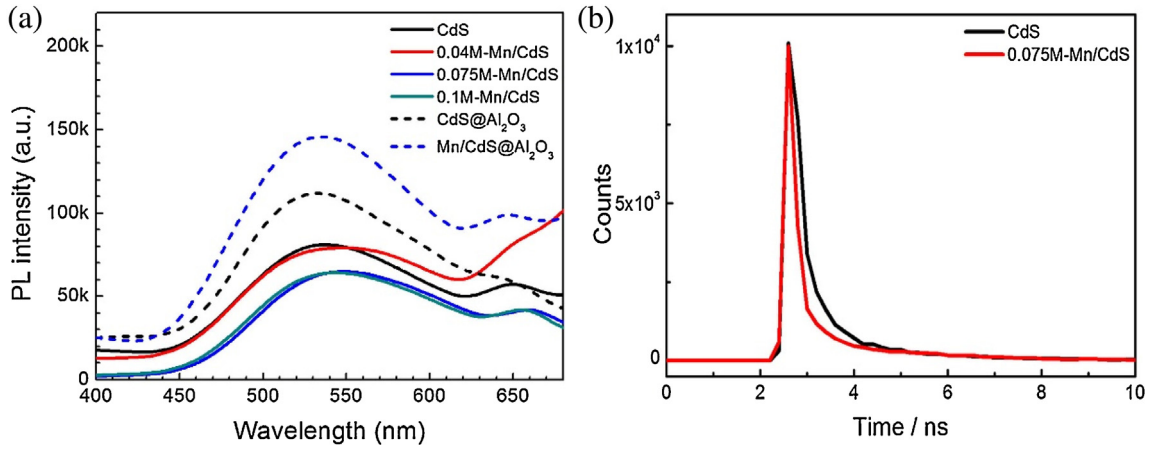

Fig. 5. (a) Photoluminescence (PL) curves and (b) excited state electron radiative decay of the TiO_2 films loaded with undoped and Mn-doped CdS QDs, respectively. (Excitation wavelength 325 nm).

film with increase of Mn dopant. In all cases, the relative content of Cd + S + Mn is ~7%. EDS is only considered as an observation measurement, which is difficult to monitor the accurate variation of the elements content when the content of element is low. The total content of Cd, S and Mn elements is no more than 8% so that the bias of measurement covers up the variation of the contents. The increased amount of QDs mainly results from the increase of nucleation number in the formation process of QDs. The possible reason is that Mn^{2+} in the precursor solution boost the nucleation of QDs according to the principle of heterogeneous nucleation [39,40]. But it is difficult to find a good testing method to verify this conclusion. However, the increase of the absorption region (red-shift) is another story. According to the previous work [33], the band gaps of the QDs are calculated to be 2.14 eV for CdS, 2.10 eV for 0.04 M-Mn/CdS, 2.05 eV for 0.075 M-Mn/CdS, and 2.07 eV for 0.1 M-Mn/CdS as shown in Fig. 2(b). The decrease of band gap for Mn-doped CdS QDs may be attributed to the formation of Mn mid-gap in CdS band gap [34,41]. According to the results of the light absorbance, LHE will be increased by doping Mn^{2+} into CdS QDs.

To verify the conclusion, the LHE characteristics of the QDSCs assembled with CdS QDs with and without Mn dopant were measured as shown in Fig. 3. The value of the LHE is calculated by the following equation [42]:

$$\mathrm{LHE} = \frac{A(QD)}{A(TiO2 + QD)}\left(1 - 10^{-(A_{(TiO2+QD)} * d)}\right) \quad (2)$$

where $A_{(QD)}$ and $A_{(TiO2+QD)}$ are the absorbance of the TiO_2 films prior to and following QDs absorption, respectively. d is the thickness of films. The LHE of Mn/CdS based QDSCs is strongly higher than that of the case made by CdS, from 400 nm to 600 nm. LHE of QDSCs can be enhanced by doping Mn^{2+} into CdS QDs, which is helpful for high-generated current density of the solar cells.

It is well known that the charge generation and collection of the solar cell can be evaluated by incident photon to charge carrier efficiency (IPCE) and absorbed photon to current conversion efficiency (APCE). In the closed circuit, the definition of IPCE is the ratio of the electron number and the incident monochromatic photon number Per unit time. IPCE value is also affected by three parts: LHE, Φ_{inj} and η_{cc}. It is expressed by the following equation [43]:

$$\mathrm{IPCE} = \mathrm{LHE} \times \Phi_{inj} \times \eta_{cc} \quad (3)$$

The APCE is calculated by the following equation [42]:

$$\mathrm{APCE} = \Phi_{inj} \times \eta_{cc} = \frac{IPCE}{LHE} = \frac{IPCE}{\frac{A(QD)}{A(QD+TiO2)}\left(1 - 10 - (A(QD + TiO2) * d)\right)} \quad (4)$$

Fig. 4(a) shows IPCE spectra of the solar cells. It can be seen that the IPCE values of Mn-doped devices are higher than that of device

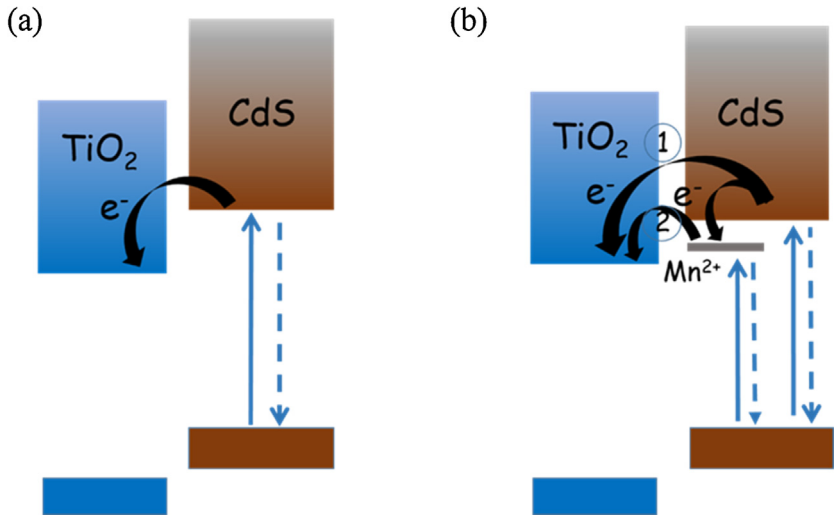

Scheme 2. Energy band structures of TiO_2/CdS (Mn/CdS).

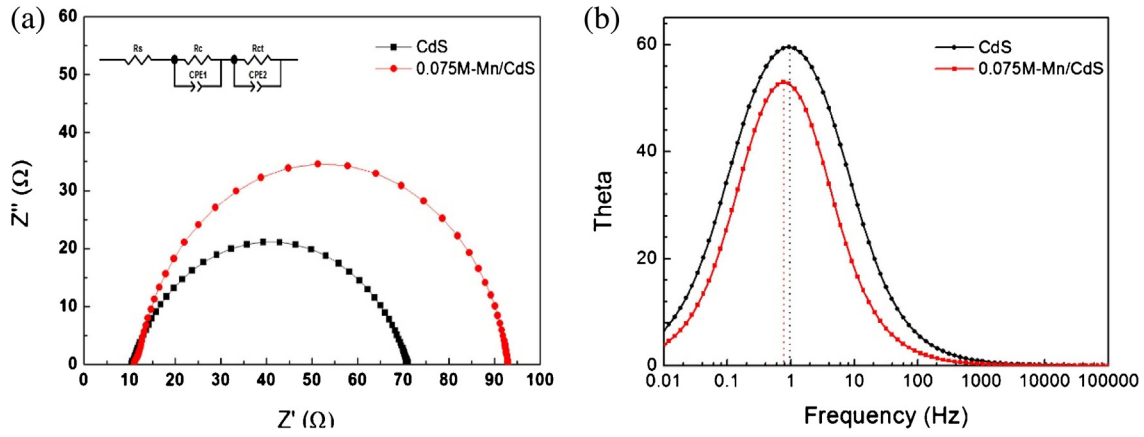

Fig. 6. (a) Nyquist plot curves and (b) Bode plot curves of the QDSCs assembled with CdS and 0.075 M-Mn/CdS QDs under forward bias (-0.6 V) and dark condition.

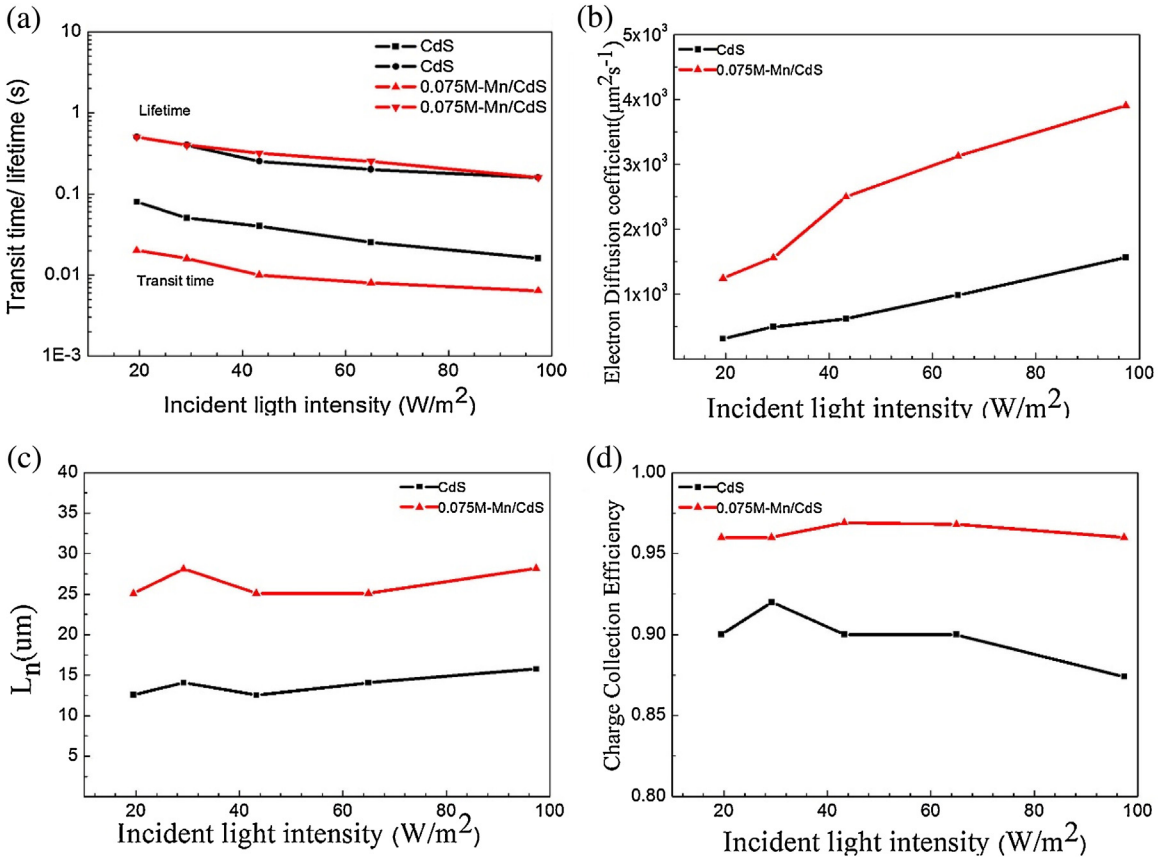

Fig. 7. (a) Electron transport time and electron lifetime, (b) Electron diffusion coefficient, (c) Electron diffusion length and (d) Effective charge collection efficiency of the QDSCs assembled with CdS and 0.075 M-Mn/CdS QDs as a function of the incident light intensity.

without dopant. The 0.075 M-Mn/CdS sample shows the highest IPCE value. The IPCE spectra of Mn/CdS sample is red shifted in comparison with CdS sample. Such characteristics exhibit the same trend as the UV-visible spectra and *J-V* curves (Fig. 1 and Fig. 2). To better understand the role of Mn dopant on the electron injection and collection, APCE for both CdS and Mn/CdS QDSCs have been measured as shown in Fig. 4(b). The APCE value of the 0.075 M-Mn/CdS based solar cell is higher than that of sample without Mn dopant in the wavelength range of more than 480 nm. It demonstrates that Mn dopant can improve the efficiency of the conversion of the absorbed photons, although the APCE value has no obvious increase in the short wavelength (<480 nm). It is clear that the increase of the J_{sc} depends on not only the high light harvesting efficiency but also the charge collection and injection efficiencies.

We have further probed the relative energy position of the quantum dots (both undoped and Mn-doped CdS) from where the electron gets injected to the TiO_2 conduction band by monitoring the electron injection rate using Photoluminescence spectroscopy as shown in Fig. 5(a). In addition, a blocking layer of Al_2O_3 on the surface of TiO_2 films is introduced to verify the number of the excited electrons of QDs with and without Mn dopant [44]. There is an obvious peak around 650 nm in every curve of Fig. 5(a), which is frequency doubling peak (the excited wavelength is 325 nm) and does not influence the analysis of experimental result. The PL emission of Mn^{2+} does not appear in the spectra, because the overall PL emission of Mn-doped QDs is donated by QDs excited emission [45]. It can be seen that PL intensity of photoanode loaded with Mn/CdS QDs is lower than that of photoanode loaded with CdS QDs. 0.075 M-Mn/CdS QDs photoanode exhibits the lowest PL intensity. The PL emission intensity is markedly quenched despite the increase in the absorption intensity after Mn^{2+} doping into CdS QDs. So excitions are effectively separate into electrons–holes. And then the electrons transfer to TiO_2 conduction band. Thus, Mn dopant can delay the charge recombination. The PL intensity of the TiO_2 films coated Al_2O_3 layer is higher than that of the untreated films because the blocking layer of Al_2O_3 hinders the electrons transition to TiO_2 and increases radiative recombination fluorescence. Therefore, more excitied electron and faster injection rate can be obtained by doping Mn^{2+} into CdS QDs. To prove the increase of injection kinetics of doped QDs, the excited state electron radiative decay of the photoanodes is measured as shown in Fig. 5(b). The short-lived excited state means the injection rate of electrons in the semiconductor is increased [46,47]. Fig. 5(b) shows a clear increase in electron injection rate after doping Mn^{2+} into CdS QDs. Thus, the Mn dopant can accelerate the electron injection from QDs to TiO_2 and reduce the electron-hole recombination. Scheme 2 displays the energy band structures of TiO_2/CdS and TiO_2/Mn/CdS. It demonstrates that the excited electrons on conduction band of QDs inject into conduction band of TiO_2 through two ways (①, ②). Although the electron transport distance from CdS conduction band to TiO_2 conduction band is extended by Mn mid gap, the faster speed of electron transport improves the electron collection.

Fig. 6 displays the electrochemical impedance spectra (EIS) of the QDSCs measured under dark condition with forward a bias of -0.6 V. The fitting impedance results of Fig. 6 are listed in Table 3. Nyquist curves obtained from EIS measurements are fitted the

equivalent circuit model as shown in Fig. 6(a). The intercept of high frequency and the horizontal ordinate is the ohm resistance (R_s), related to the surface of working electrode base resistance. The high frequency semicircle (R_c) shows the transport resistance at the counter electrode and electrolyte interface. The intermediate frequency semicircle (R_{ct}) is associated with the interface resistance of TiO_2/QD/electrolyte. The values of R_{ct} corresponding to CdS and Mn/CdS samples are 68.5 Ω and 80.5 Ω, respectively, which means the electrons and holes of the Mn-doped CdS solar cells are more difficult to recombine in the electrolyte than that of CdS devises. Thus, the less charge recombination can be emerged in Mn/CdS QDSC. The corresponding Bode phase plots for cells with Mn-doped and undoped are shown in Fig. 6(b). The electron lifetimes (τ_r) can be obtained according to the following equation [48]:

$$\tau_r = 1/(2\pi f_{max}) \quad (5)$$

where f_{max} is the maximum frequency in the Bode plot. The τ_r values of CdS and 0.075 M Mn-CdS devices are found to be 0.17 s and 0.21 s, respectively. The higher τ_r value of Mn/CdS means that electrons have a longer lifetime. The result that the employment of the Mn dopant in CdS enhances the charge recombination resistance. So the Mn dopant in CdS can reduce the charge recombination and prolong the electron lifetime of the solar cell, which is agreement in the result of PL spectra. In order to further characterize the electron transport and charge recombination of the QDSCs based on CdS and Mn/CdS QDs, intensity modulated photocurrent spectroscopy (IMPS) and intensity modulated photovoltage spectroscopy (IMVS) have been tested. The conducted light intensities are changed from 19.48 to 97.38 Wm^{-2}. The values of the electron transit time (τ_d) and electron lifetime (τ_r) can be calculated by the following equations [48–50]:

$$\tau_d = 1/2\pi f_d \quad (6)$$

$$\tau_r = 1/2\pi f_r \quad (7)$$

where f_d and f_r are the characteristic frequency minimum of the IMPS and IMVS imaginary component, respectively. Fig. 7(a) shows that the transit time of Mn/CdS sample is much lower than that of CdS sample. In term of the PL results, the introduction of Mn mid-gap can boost the electron injection and transport. In addition, the electron lifetime has an obvious increase which is consisted with the result of the Bode plot curve [48]. The more details can be obtained from Fig. 7(b-d). The electron diffusion coefficient (D_n) can be described by the following equation [49–51]:

$$D_n = d^2/2.35\tau_d \quad (8)$$

The electron diffusion length (L_n) and electron collection efficiency (η_{cc}) can be calculated by the following equations [51,52]:

$$L_n = (D_n\tau_r)^{1/2} \quad (9)$$

$$\eta_{cc} = 1 - \tau_d/\tau_r \quad (10)$$

In view of the results, both the electron transition rate and the electron diffusion length are increased by doping Mn^{2+} into CdS QDs, which results in the enhancement of η_{cc}, from 89.9% for CdS device to 96.7% for Mn/CdS device.

Photovoltaic parameters have been gathered from sixteen cells and statistical analysis of the result is shown in Fig. 8. It can be seen that the Mn/CdS devices show good reproducibility with a high efficiency (>3%), which is much higher that of CdS devices (~2%). According to all of discussion, the increase of PCE for Mn/CdS QDSCs is mainly derived from the enhancement of the light harvesting efficiency (LHE) and collection efficiency at the back contact (η_{cc}).

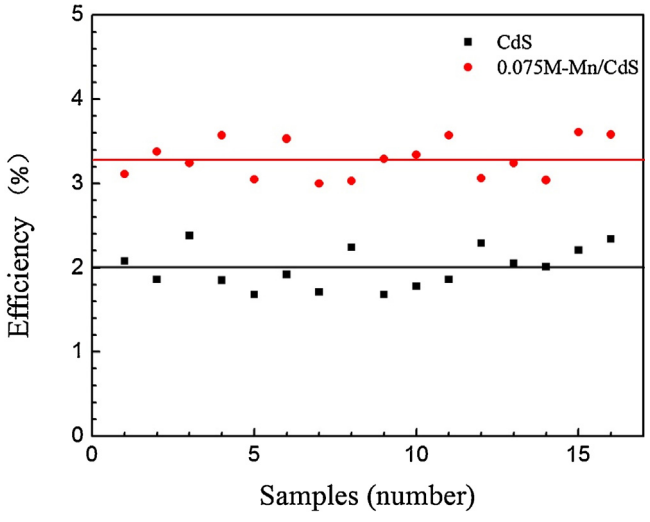

Fig. 8. Distribution of sixteen cells' efficiency, the lines representative the average PCE of the solar cells assembled with CdS and 0.075 M-Mn/CdS QDs, respectively.

4. Conclusions

Mn^{2+} doped CdS QDSCs were obtained by successive ionic layer absorption and reaction (SILAR) method. The power conversion efficiency (PCE) of Mn/CdS device was up to 3.29% when the concentration of Mn^{2+} precursor solution was 0.075 M, which is much higher than that of CdS device (2.01%). We found that the Mn dopant into CdS QDs increased the light absorbance and extended the light absorption range, which resulted in the enhancement of the light harvesting efficiency (LHE). In addition, the faster speed of electron transport and longer electron diffusion length for Mn/CdS QDs devices improved the charge collection efficiency (η_{cc}) of the solar cells. η_{cc} was increased from 89.9% for CdS device to 96.7% for Mn/CdS device. As a result, the improvement of PCE for Mn/CdS QDSCs was mainly derived from the enhancement of LHE and η_{cc}.

ACKNOWLEDGMENTS

This work was supported by the National Science Foundation of China (51374029, 5151101345), Program for New Century Excellent Talents in University (NCET-13-0668), Fundamental Research Funds for the Central Universities (FRF-TP-14-008C1). This work was also supported by the "thousands talents" program for the pioneer researcher and his innovation team, China.

References

[1] J.Y. Kim, O. Voznyy, D. Zhitomirsky, E.H. Sargent, 25th anniversary article: Colloidal quantum dot materials and devices: A quarter-century of advances, Adv. Mater. 25 (2013) 4986–5010.
[2] A. Salant, M. Shalom, I. Hod, A. Faust, A. Zaban, U. Banin, Quantum dot sensitized solar cells with improved efficiency prepared using electrophoretic deposition, ACS nano 4 (2010) 5962–5968.
[3] A. Aboulaich, D. Billaud, M. Abyan, L. Balan, J.J. Gaumet, G. Medjadhi, J. Ghanbaja, R. Schneider, One-pot noninjection route to CdS quantum dots via hydrothermal synthesis, ACS Appl. Mater. Interfaces 4 (2012) 2561–2569.
[4] J.H. Rhee, C.C. Chung, E.W.G. Diau, A perspective of mesoscopic solar cells based on metal chalcogenide quantum dots and organometal-halide perovskites, NPG Asia Mater. 5 (2013) 1–17.
[5] X. Wang, G.I. Koleilat, J. Tang, H. Liu, I.J. Kramer, R. Debnath, L. Brzozowski, D.A. R. Barkhouse, L. Levina, S. Hoogland, E.H. Sargent, Tandem colloidal quantum dot solar cells employing a graded recombination layer, Nat. Photo. 5 (2011) 480–484.

[6] H.W. Hillhouse, M.C. Beard, Solar cells from colloidal nanocrystals: Fundamentals, materials, devices, and economics, Curr. Opin. Colloid Interface Sci. 14 (2009) 245–259.
[7] M.C. Acuna, S.B. Ruiz, C.R.M. Figueroa, R.C. Acuna, O.J.P. Perez, Synthesis characterization and evaluation of the cytotoxicity of Ni-doped Zn(Se, S) quantum dots, J. Nanomater. 2015 (2015) 1–8.
[8] O. Chen, J. Zhao, V.P. Chauhan, J. Cui, C. Wong, D.K. Harris, H. Wei, H. Han, D. Fukumura, R.K. Jain, M.G. Bawendi, Compact high-quality CdSe-CdS core-shell nanocrystals with narrow emission linewidths and suppressed blinking, Nat. Mater. 12 (2013) 445–451.
[9] S. Li, Q. Gong, C. Cao, X. Wang, J. Yan, Y. Wang, H. Wang, A review of external cavity-coupled quantum dot lasers, Opt. Quant. Electron. 46 (2014) 623–640.
[10] M.B. Wilker, K.J. Schnitzenbaumer, G. Dukovic, Recent progress in photocatalysis mediated by colloidal II-VI nanocrystals, Isr. J. Chem. 52 (2012) 1002–1015.
[11] K. Sun, M. Vasudev, H.-S. Jung, J. Yang, A. Kar, Y. Li, K. Reinhardt, P. Snee, M.A. Stroscio, M. Dutta, Applications of colloidal quantum dots, Microelectron. J. 40 (2009) 644–649.
[12] P.V. Kamat, Quantum dot solar cells. Semiconductor nanocrystals as light harvesters, J. Phys. Chem. C 112 (2008) 18737–18753.
[13] M.R. Kim, D. Ma, Quantum-dot-based solar cells: Recent advances, strategies, and challenges, J. Phys. Chem. Lett. 6 (2015) 85–99.
[14] W. Yu, L. Qu, W. Guo, X. Peng, Experimental determination of the extinction coefficient of CdTe, CdSe and CdS nanocrystals, Chem. Mater. 15 (2003) 2854–2860.
[15] M. Gratzel, Photoelectrochemical cells, Nature 414 (2001) 338–344.
[16] W.A. Tisdale, K.J. Williams, B.A. Timp, D.J. Norris, E.S. Aydil, X. Zhu, Hot-electron transfer from semiconductor nanocrystals, Science 328 (2010) 1543–1547.
[17] O.E. Semonin, J.M. Luther, S. Choi, H. Chen, J. Gao, A.J. Nozik, M.C. Beard, Peak external photocurrent quantum efficiency exceeding 100% via MEG in a quantum dot solar cell, Science 334 (2011) 1530–1533.
[18] R.J. Ellingson, M.C. Beard, J.C. Johnson, P.R. Yu, O.I. Micic, A.J. Nozik, A. Shabaev, A.L. Efros, Highly efficient multiple exciton generation in colloidal PbSe and PbS quantum dots, Nano Lett. 5 (2005) 865–871.
[19] A.J. Nozik, Multiple exciton generation in semiconductor quantum dots, Chem. Phys. Lett. 457 (2008) 3–11.
[20] W. Shockley, Field-enhanced donor diffusion in degenerate semiconductor layers, J. Appl. Phys. 32 (1961) 1402–1403.
[21] A.J. Nozik, Exciton multiplication and relaxation dynamics in quantum dots: applications to ultrahigh-efficiency solar photon conversion, Inorg. Chem. 44 (2005) 6893–6899.
[22] P.V. Kamat, Quantum dot solar cells. The next big thing in photovoltaics, J. Phys. Chem. Lett. 4 (2013) 908–918.
[23] W. Li, X. Zhong, Capping ligand-induced self-assembly for quantum dot sensitized solar cells, J. Phys. Chem. Lett. 6 (2015) 796–806.
[24] J. Tian, G. Cao, Control of nanostructures and interfaces of metal oxide semiconductors for quantum-dots-sensitized solar cells, J. Phys. Chem. Lett. 6 (2015) 1859–1869.
[25] J. Tian, R. Gao, Q. Zhang, S. Zhang, Y. Li, J. Lan, X. Qu, G. Cao, Enhanced performance of CdS/CdSe quantum dot cosensitized solar cells via homogeneous distribution of quantum dots in TiO_2 film, J. Phys. Chem. C 116 (2012) 18655–18662.
[26] B. Gao, C. Shen, S. Yuan, B. Zhang, M. Zhang, Y. Yang, G. Chen, Influence of nanocrystal size on the quantum dots sensitized solar cells' performance with low temperature synthesized CdSe quantum dots, J. Alloys Compd. 612 (2014) 323–329.
[27] Y.L.C. Lee, C. Hsiu, Efficient polysulfide electrolyte for CdS quantum dot-sensitized solar cells, J. Power Sources 185 (2008) 584–588.
[28] C. Chuang, P.R. Brown, V. Bulovic, M.G. Bawendi, Improved performance and stability in quantum dot solar cells through band alignment engineering, Nat. Mater. 13 (2014) 796–801.
[29] Z. Pan, H. Zhang, K. Cheng, Y. Hou, J. Hua, X. Zhong, Highly efficient inverted Type-I CdS/CdSe core/shell structure QD-sensitized solar cells, ACS Nano 6 (2012) 3982–3991.
[30] J.G. Radich, R. Dwyer, P.V. Kamat, Cu_2S reduced graphene oxide composite for high-efficiency quantum dot solar cells. Overcoming the redox limitations of S^{2-}/S_n^{2-} at the counter electrode, J. Phys. Chem. Lett. 2 (2011) 2453–2460.
[31] J. Tian, Q. Zhang, E. Uchaker, R. Gao, X. Qu, S. Zhang, G. Cao, Architectured ZnO photoelectrode for high efficiency quantum dot sensitized solar cells, Energy Environ. Sci. 6 (2013) 3542–3547.
[32] J. Tian, Q. Zhang, E. Uchaker, Z. Liang, R. Gao, X. Qu, S. Zhang, G. Cao, Constructing ZnO nanorod array photoelectrodes for highly efficient quantum dot sensitized solar cells, J. Mater. Chem. A 1 (2013) 6770–6775.
[33] J. Tian, Q. Zhang, L. Zhang, R. Gao, L. Shen, S. Zhang, X. Qu, G. Cao, ZnO/TiO_2 nanocable structured photoelectrodes for CdS/CdSe quantum dot co-sensitized solar cells, Nanoscale 5 (2013) 936–943.
[34] P.K. Santra, P.V. Kamat, Mn-doped quantum dot sensitized solar cells: A strategy to boost efficiency over 5%, J. Am. Chem. Soc. 134 (2012) 2508–2511.
[35] J. Tian, L. Lv, C. Fei, Y. Wang, X. Liu, G. Cao, A Highly efficient (>6%) $Cd_{1-x}Mn_xSe$ quantum dot sensitized solar cell, J. Mater. Chem. A 2 (2014) 19653–19659.
[36] C.V.V.M. Gopi, M.V. Haritha, S.K. Kim, H.J. Kim, A strategy to improve the energy conversion efficiency and stability of quantum dot-sensitized solar cells using manganese-doped cadmium sulfide quantum dots, Dalton Trans. 44 (2015) 630–638.
[37] T. Ma, S. Yun, Dye-sensitized solar cells-theoretical basis to technical application, Chemical Industry Press, Beijing, 2016, pp. 25.
[38] M.V. Haritha, C.V.V.M. Gopi, C.V.T. Varma, S.-K. Kim, H.-J. Kim, Influence of Mn^{+2} incorporation in CdSe quantum dots for high performance of CdS–CdSe quantum dot sensitized solar cells, J. Photochem. Photobiol. A 315 (2016) 34–41.
[39] X. Guo, H. Dong, G. Niu, Y. Qiu, L. Wang, Mg doping in nanosheet-based spherical structured ZnO photoanode for quasi-solid dye-sensitized solar cells, RSC Adv. 4 (2014) 21294–21300.
[40] D. Zhang, L. Sun, J. Zhang, Z. Yan, C. Yan, Hierarchical construction of ZnO architectures promoted by heterogeneous nucleation, Cryst. Growth Des. 8 (2008) 3609–3615.
[41] P.K. Santra, Y. Chen, Role of Mn^{2+} in Doped Quantum Dot Solar Cell, Electrochim. Acta 146 (2014) 654–658.
[42] S. Power, Q. Wu, M. Weidelener, A. Nattestad, Z. Hu, A. Mishra, P. Bauerle, L. Spiccia, Y. Cheng, U. Bach, Improved photocurrents for p-type dye-sensitized solar cells using nano-structured nickel(II) oxide microballs, Energy Environ. Sci. 5 (2012) 8896–8900.
[43] J. Huang, B. Xu, C. Yuan, H. Chen, J. Sun, L. Sun, H. Agren, Improved performance of colloidal CdSe quantum dot-sensitized solar cells by hybrid passivation, ACS Appl. Mater. Interfaces 6 (2014) 18808–18815.
[44] J.N. Schrauben, Y. Zhao, C. Mercado, P.I. Dron, J. Michl, K. Zhu, J.C. Johnson, Photocurrent enhanced by singlet fission in a dye-sensitized solar cell, ACS Appl. Mater. Interfaces 7 (2015) 2286–2293.
[45] R. Beaulac, P.I. Archer, X.Y. Liu, S. Lee, G.M. Salley, M.G. Dobrowolska, J. k. Furdyna, D.R. Gamelin, Spin-polarizable excitonic luminescence in colloidal Mn^{2+}-doped CdSe quantum dots, Nano Lett. 8 (2008) 1197–1201.
[46] P.R.F. Barnes, A.Y. Anderson, S.E. Koops, J.R. Durrant, B.C. O'Regan, Electron injection efficiency and diffusion length in dye-sensitized solar cells derived from incident photon conversion efficiency measurements, J. Phys. Chem. C 113 (2009) 1126–1136.
[47] K.B. Zheng, K. Karli, K. Zidek, T. pullerits, Ultrafast photoinduced dynamics in quantum dot-based systems for light harvesting, Nano Res. 8 (2015) 2125–2142.
[48] R. Kern, R. Sastrawan, J. Ferber, R. Stangl, J. Luther, Modeling and interpretation of electrical impedance spectra of dye solar cells operated under open-circuit conditions, Electrochim. Acta 47 (2002) 4213–4225.
[49] S. Nakade, T. Kanzaki, Y. Wada, S. Yanagida, Stepped light-induced transient measurements of photocurrent and voltage in dye-sensitized solar cells: Application for highly viscous electrolyte systems, Langmuir 21 (2005) 10803–10807.
[50] J. van de Lagemaat, A.J. Frank, Nonthermalized electron transport in dye-sensitized nanocrystalline TiO_2 films: transient photocurrent and random-walk modeling studies, J. Phys. Chem. B 105 (2001) 11194–11205.
[51] Y. Wang, K. Li, Y. Xu, H. Rao, C. Su, D. Kuang, Hydrothermal fabrication of hierarchically macroporous Zn_2SnO_4 for highly efficient dye-sensitized solar cells, Nanoscale 5 (2013) 5940–5948.
[52] Q. Wang, J.E. Moser, M. Gratzel, Electrochemical impedance spectroscopic analysis of dye-sensitized solar cells, J. Phys. Chem. B 109 (2005) 14945–14953.